Role of protein fluctuation correlations in electron transfer in photosynthetic complexes

Alexander I. Nesterov*
Departamento de Física, CUCEI, Universidad de Guadalajara, Avenida Revolución 1500, Guadalajara, Codigo Postal 44420, Jalisco, Mexico

Gennady P. Berman†
Theoretical Division, T-4, Los Alamos National Laboratory and the New Mexico Consortium, Los Alamos, New Mexico 87544, USA
(Received 25 November 2014; published 6 April 2015)

We consider the dependence of the electron transfer in photosynthetic complexes on correlation properties of random fluctuations of the protein environment. The electron subsystem is modeled by a finite network of connected electron (exciton) sites. The fluctuations of the protein environment are modeled by random telegraph processes, which act either collectively (correlated) or independently (uncorrelated) on the electron sites. We derived an exact closed system of first-order linear differential equations with constant coefficients, for the average density matrix elements and for their first moments. Under some conditions, we obtained analytic expressions for the electron transfer rates and found the range of parameters for their applicability by comparing with the exact numerical simulations. We also compared the correlated and uncorrelated regimes and demonstrated numerically that the uncorrelated fluctuations of the protein environment can, under some conditions, either increase or decrease the electron transfer rates.

DOI: 10.1103/PhysRevE.91.042702 PACS number(s): 87.15.ht, 82.39.Jn, 03.65.Yz, 05.60.Gg

I. INTRODUCTION

In a photosynthetic organism, sunlight is absorbed in the light-harvesting complex or antenna, by a light-sensitive (chlorophyll or carotenoid) molecule. This is the first step in transforming solar energy into electron energy in the form of the exciton. This exciton travels through many connected sites (pigments) of the antenna complex, and finally reaches the reaction center where charge separation and chemical reactions take place. (See, for example, [1,2], and references therein.)

The time scale of the primary processes of electron (exciton) transfer (ET) and charge separation are very fast, $t_{\text{prime}} \approx 1$–$3$ ps. There are two major theoretical challenges in describing these primary processes. The first problem is that the constant of interaction λ_n between the electron site n and the protein environment is usually not small. Indeed, the well-known Marcus formula for the ET rate k_{da} between the donor and the acceptor, under the influence of the collective protein thermal fluctuations, has the form [3,4] $k_{da} = (2\pi|V_{da}|^2/\sqrt{4\pi\varepsilon_r T})\exp[-(\varepsilon-\varepsilon_r)^2/4k_B T\varepsilon_r]$. Here ε is the difference between the donor and the acceptor site energies, V_{da} is the matrix element of the donor-acceptor interaction, T is the absolute temperature, k_B is the Boltzmann constant, and ε_r is the so-called reconstruction energy, $\varepsilon_r \propto \lambda^2$. As one can see, the interaction constant λ occurs in the denominators of both the preexponential factor and in the exponent. This result cannot be obtained by using standard perturbative approaches by expanding the initial expressions in a power series in the interaction constant λ.

It is known that the Marcus formula is derived in the high-temperature limit but can also be used for room temperature [4]. A significant development of the Marcus theory was achieved in [5,6], where the extensions for a wide range of temperatures and for different properties of a solvent were incorporated. Note that in [3–6] a single protein environment was used which acts on both donor and acceptor, but with different coupling constants. However, the important question remains: What modifications for the ET process will occur if a combination of correlated and independent (uncorrelated) protein environments acts on different electron sites?

In [7,8], stochastic models, with uncorrelated noises acting on different sites, were used to elucidate the unidirectionality of the primary charge separation process in bacterial reaction centers with two symmetric methods of ET, starting from the common electron donor. These papers addressed the well-known problem of highly asymmetric ET in photosynthetic reaction centers.

Note that, in real photosynthetic organisms, uncorrelated protein fluctuations can act on their neighboring pigments as well as on other pigments. Experimentally, this can be verified by measuring the corresponding correlation functions of the protein fluctuations between different donor-acceptor sites. The correlation properties of protein fluctuations at different electron sites can also be modeled and simulated numerically using standard molecular dynamics approaches.

In [9,10], we introduced a quantum mechanical nonperturbative model to describe multilevel donor-acceptor systems. The model was used to describe multiscale ET dynamics and nonphotochemical quenching by a charge transfer state in photosynthetic biocomplexes. In our approach the protein environment is modeled by a random telegraph process (RTP).

In this paper, we extend our model to the case in which the random protein environment can act both collectively and independently on all light-sensitive electron sites (pigments). Namely, for all electron sites, we introduce both collective (correlated) and independent (uncorrelated) protein fluctuations, modeled by RTP's. We apply our model to determine the quantum ET dynamics of the simplest donor-acceptor system. Our main goal is to clarify the similarities and differences in the actions of correlated and uncorrelated protein environments

*nesterov@cencar.udg.mx
†gpb@lanl.gov

on the ET processes. Under some conditions, we derived analytic expressions for the ET rates that are a generalization of the Marcus-type expression for a noisy protein environment. We compared our analytic expressions, in a wide range of parameters, with the results of exact numerical simulations. We demonstrated numerically that the uncorrelated fluctuations of the protein environment can either increase or decrease the ET rates.

Although protein environments modeled by random processes and by the thermal bath usually produce different long-time asymptotic behavior for the ET dynamics, we believe that our approach is appropriate for problems when the stationary states are realized before thermal equilibrium is approached [8,10]. Note also that protein environments in living organisms have both noisy and thermal components [3,4,7,8,11–21].

The structure of the paper is as follows. In Sec. II, we describe our model, and derive the closed system of differential equations for the averaged density matrix elements and for their moments. In Sec. III, we apply our approach to a specific "donor-acceptor" system, introduce the characteristic parameters, and present the results of the numerical simulations for both the exact and approximate solutions. In the Conclusion, we summarize our results and formulate some challenges for future research. In the Supplemental Material [22], we present mathematical details of our approach, and additional illustrations of the actions of correlated and uncorrelated protein environments on the ET.

II. DESCRIPTION OF THE MODEL

Consider a quantum system which is described by a time-dependent Hamiltonian $\mathcal{H}(t)$. We assume that this Hamiltonian depends on some control parameters λ_a. The noise associated with fluctuations of these parameters is described by the functions $\delta\lambda_a(t)$, which depend on the random variables $\xi_a(t)$. Expanding the Hamiltonian to first order in $\xi_a(t)$, we have

$$\mathcal{H}(t) = \mathcal{H}_0 + \sum_a \mathcal{V}_a \xi_a(t), \tag{1}$$

where $\mathcal{H}_0$, is the Hamiltonian of the system under consideration, and $\mathcal{V}_a$ is a matrix that describes the interaction with noise. Using (1), we obtain the following equations of motion for the density matrix ($\hbar = 1$):

$$\frac{d\rho}{dt} = i[\rho,\mathcal{H}_0] + i\left[\rho, \sum_a \mathcal{V}_a,\xi_a(t)\right]. \tag{2}$$

For the density matrix averaged over noise this yields

$$\frac{d\langle\rho\rangle}{dt} = i[\langle\rho\rangle,\mathcal{H}_0] + i\sum_a [\langle\rho\xi_a(t)\rangle,\mathcal{V}_a], \tag{3}$$

where the average $\langle\cdots\rangle$ is taken over the random processes.

To close this system of differential equations (3), we assume that the fluctuations are produced by the independent random telegraph processes

$$\langle\xi_a(t)\rangle = 0, \tag{4}$$

$$\langle\xi_a(t)\xi_b(t')\rangle = \delta_{ab}\sigma_a^2 e^{-2\gamma_a\tau}. \tag{5}$$

Employing the differential formula for the RTP [23],

$$\left(\frac{d}{dt} + 2\gamma_a\right)\langle\xi_a(t)R[t;\xi_a(\tau)]\rangle = \left\langle\xi_a(t)\frac{d}{dt}R[t;\xi_a(\tau)]\right\rangle, \tag{6}$$

where $R[t;\xi_a(\tau)]$, is an arbitrary functional, we obtain from Eq. (3) the following system of differential equations:

$$\frac{d\langle\rho\rangle}{dt} = i[\langle\rho\rangle,\mathcal{H}_0] + i\sum_a \sigma_a[\langle X_a\rangle,\mathcal{V}_a], \tag{7}$$

$$\frac{d\langle X_a\rangle}{dt} = i[\langle X_a\rangle,\mathcal{H}_0] + i\sigma_a[\langle\rho\rangle,\mathcal{V}_a] + i\sum_{b\neq a}\sigma_b[\langle X_{ab}\rangle,\mathcal{V}_b] - 2\gamma_a\langle X_a\rangle, \tag{8}$$

$$\frac{d\langle X_{ab}\rangle}{dt} = i[\langle X_{ab}\rangle,\mathcal{H}_0] + i\sigma_a[\langle X_b\rangle,\mathcal{V}_b] + i\sigma_b[\langle X_a\rangle,\mathcal{V}_b] - 2(\gamma_a+\gamma_b)\langle X_{ab}\rangle, \tag{9}$$

where $\langle X_a(t)\rangle = \langle\xi_a(t)\rho(t)\rangle/\sigma_a$ and $\langle X_{ab}(t)\rangle = \langle\xi_a(t)\xi_b(t)\rho(t)\rangle/(\sigma_a\sigma_b)$ $(a \neq b)$. Not, that by using the properties of the RTP, one can show that $\langle X_{aa}(t)\rangle = \langle\rho(t)\rangle$. Therefore, the diagonal elements of the matrix $\langle X_{ab}(t)\rangle$ do not add new equations to the system (7)–(9).

In the rest of this paper, we use Eqs. (7)–(9) to study the two-level donor-acceptor system (TLS) embedded in a noisy protein environment. We assume that two uncorrelated RTPs (generally with different interaction constants) act one each on the donor and the acceptor.

III. TWO-LEVEL DONOR-ACCEPTOR SYSTEM

For simplicity of consideration, we apply our approach to a TLS with the following Hamiltonian:

$$\tilde{\mathcal{H}} = \sum_n \varepsilon_n|n\rangle\langle n| + \sum_{m\neq n} V_{mn}|m\rangle\langle n| + \sum_{m,n}\lambda_{mn}(t)|m\rangle\langle n|, \quad m,n = 0,1, \tag{10}$$

where the functions $\lambda_{mn}(t)$ describe the influence of noise. When the matrix elements V_{nm} are absent, the diagonal matrix elements $\lambda_{nn}(t)$ are responsible for decoherence—the decay of the nondiagonal density matrix elements. When $\lambda_{mn}(t) = 0$ $(m \neq n)$, relaxation in the system occurs only if $V_{mn} \neq 0$. When $V_{mn} = 0$, the off-diagonal matrix elements $\lambda_{mn}(t)$ $(m \neq n)$ lead to "direct" relaxation processes.

In what follows, we restrict ourselves to diagonal noise effects produced by two independent (uncorrelated) protein environments described by the RTPs $\xi_{1,2}(t)$. Then one can write $\lambda_{mn}(t) = \delta_{mn}\sum_{a=1}^{2}\lambda_n^{(a)}\xi_a(t)$, where $\lambda_n^{(a)}$ is the interaction constant with the ath environment $\xi_a(t)$ at the site n $(a,n = 1,2)$. Note that, in our approach, each noise can act on both donor and acceptor sites. (See Fig. 1.) The limit of a single collective noise, acting on both the donor and acceptor sites, corresponds to $\lambda_{1,2}^{(1)} \neq 0$ and $\lambda_{1,2}^{(2)} = 0$, or $\lambda_{1,2}^{(1)} = 0$ and $\lambda_{1,2}^{(2)} \neq 0$. The limit of two uncorrelated noises, acting one

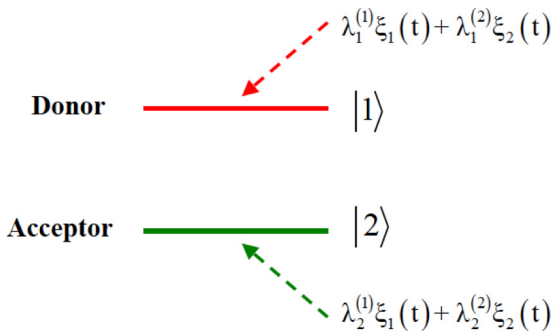

FIG. 1. (Color online) The two-level donor-acceptor system interacting with two uncorrelated noisy environments $\xi_1(t)$ and $\xi_2(t)$; $\lambda_n^{(a)}$ are the constants of interaction. The superscript $a = 1,2$ indicates the noisy environment, and the subscript $n = 1,2$ indicates the electron site.

on the donor and the other on the acceptor, corresponds to $\lambda_1^{(2)} = \lambda_2^{(1)} = 0$ or $\lambda_1^{(1)} = \lambda_2^{(2)} = 0$.

We consider the stationary telegraph noise described by the random variable $\xi_a(t) = \zeta_a(t) - \bar{\zeta}_a$, so that

$$\langle \xi_a(t)\rangle = 0, \tag{11}$$

$$\langle \xi_a(t)\xi_b(t')\rangle = \delta_{ab}\chi_a(t-t'), \tag{12}$$

where $\chi_a(t-t') = \sigma_a^2 e^{-2\gamma_a|t-t'|}$ is the correlation function of the ath noise, described by the random variable $\xi_a(t)$. The average value $\langle \zeta_a(t)\rangle = \bar{\zeta}_a$ is included in the renormalization of the electron energy at each site n in Eq. (10) as $\varepsilon_n \to \varepsilon_n + \sum_a \lambda_n^{(a)}\bar{\zeta}_a$.

A. Integro-differential equations and rates

The dynamics of the TLS can be described by the following system of integro-differential equations [19,24] (for details see [22]):

$$\frac{d}{dt}\langle\rho_{11}(t)\rangle = -\int_0^t K(t-t')[\langle\rho_{11}(t')\rangle - \langle\rho_{22}(t')\rangle]dt' + iV_{21}\langle\rho_{12}(0)\rangle - iV_{12}\langle\rho_{21}(0)\rangle, \tag{13}$$

$$\frac{d}{dt}\langle\rho_{22}(t)\rangle = \int_0^t K(t-t')[\langle\rho_{11}(t')\rangle - \langle\rho_{22}(t')\rangle]dt' - iV_{21}\langle\rho_{12}(0)\rangle + iV_{12}\langle\rho_{21}(0)\rangle, \tag{14}$$

where

$$K(t-t') = 2V^2\Phi(t-t')\cos(\varepsilon(t-t')), \tag{15}$$

$\varepsilon = \varepsilon_1 - \varepsilon_2$, and $\Phi(t-t')$ is the characteristic functional of the random process.

For the case of two uncorrelated environments described by RTPs, one can show that $\Phi(t) = \Phi_1(t)\Phi_2(t)$. The characteristic functional $\Phi_a(t)$ of each independent RTP is given by [25,26]

$$\Phi_a(t) = e^{-\gamma_a t}\left(\cosh\left(\sqrt{\gamma_a^2 - d_a^2}\,t\right) + \frac{1}{\sqrt{\gamma_a^2 - d_a^2}}\sinh\left(\sqrt{\gamma_a^2 - d_a^2}\,t\right)\right), \quad a = 1,2, \tag{16}$$

where $d_a = (\lambda_1^{(a)} - \lambda_2^{(a)})\sigma_a$ denotes the amplitude of the ath noise.

When the condition, $|\int_0^\infty \tau K(\tau)d\tau| \ll 1$, is satisfied, we can approximate Eqs. (13) and (14) by the following system of ordinary differential equations,

$$\frac{d}{dt}\langle\rho_{11}(t)\rangle = -R(t)(\langle\rho_{11}(t)\rangle - \langle\rho_{22}(t)\rangle) + iV_{21}\langle\rho_{12}(0)\rangle - iV_{12}\langle\rho_{21}(0)\rangle, \tag{17}$$

$$\frac{d}{dt}\langle\rho_{22}(t)\rangle = R(t)(\langle\rho_{11}(t)\rangle - \langle\rho_{22}(t)\rangle) - iV_{21}\langle\rho_{12}(0)\rangle + iV_{12}\langle\rho_{21}(0)\rangle, \tag{18}$$

where $R(t) = \int_0^t K(\tau)d\tau$.

Assume that initially the off-diagonal components of the density matrix (and, correspondingly, their average values) are zero, $\rho_{12}(0) = \rho_{21}(0) = 0$. Then the exact solution of Eqs. (17) and (18) can be written as

$$\langle\rho_{11}(t)\rangle = \tfrac{1}{2} + \left(\langle\rho_{11}(0)\rangle - \tfrac{1}{2}\right)e^{-2\int_0^t R(t')dt'}, \tag{19}$$

$$\langle\rho_{22}(t)\rangle = \tfrac{1}{2} + \left(\langle\rho_{22}(0)\rangle - \tfrac{1}{2}\right)e^{-2\int_0^t R(t')dt'}, \tag{20}$$

where $\langle\rho_{11}(0)\rangle = \rho_{11}(0)$ and $\langle\rho_{22}(0)\rangle = \rho_{22}(0)$. As one can see, in the limit $t \to \infty$, the presence of noise results in equal populations in the TLS.

The solution given by Eqs. (19) and (20) can be approximated by replacing $R(t)$ by its asymptotic value $\Gamma/2 = \lim_{t\to\infty} R(t)$. The result is

$$\langle\rho_{11}(t)\rangle = \tfrac{1}{2} + \left(\rho_{11}(0) - \tfrac{1}{2}\right)e^{-\Gamma t}, \tag{21}$$

$$\langle\rho_{22}(t)\rangle = \tfrac{1}{2} + \left(\rho_{22}(0) - \tfrac{1}{2}\right)e^{-\Gamma t}. \tag{22}$$

1. Two uncorrelated noises

When the environment is described by two uncorrelated RTPs, the asymptotic rate Γ is given by (see [22] for details)

$$\Gamma = \frac{2|V_{12}|^2}{\alpha_1\alpha_2(\gamma_1+\gamma_2)}\mathrm{Re}\left(\frac{(g_1 g_2-\alpha_1\alpha_2)(1+i\nu)+(\alpha_1 g_2-g_1\alpha_2)(\alpha_1-\alpha_2)}{(\alpha_1-\alpha_2)^2-(1+i\nu)^2}\right.$$
$$\left.-\frac{(g_1 g_2+\alpha_1\alpha_2)(1+i\nu)+(g_1\alpha_2+\alpha_1 g_2)(\alpha_1+\alpha_2)}{(\alpha_1+\alpha_2)^2-(1+i\nu)^2}\right), \tag{23}$$

where

$$\alpha_1=\sqrt{g_1^2-\mu_1^2},\quad \alpha_2=\sqrt{g_2^2-\mu_2^2},\quad g_1=\frac{\gamma_1}{\gamma_1+\gamma_2},\quad g_2=\frac{\gamma_2}{\gamma_1+\gamma_2},$$
$$\nu=\frac{\varepsilon}{(\gamma_1+\gamma_2)},\quad \mu_1=\frac{d_1^{(1)}-d_2^{(1)}}{\gamma_1+\gamma_2},\quad \mu_2=\frac{d_1^{(2)}-d_2^{(2)}}{\gamma_1+\gamma_2}. \tag{24}$$

In Eq. (23), we used the following notation: $d_n^{(a)}=\lambda_n^{(a)}\sigma_a$ $(a,n=1,2)$.

As was mentioned above, the condition of the applicability of Eqs. (17) and (18) is $|\int_0^\infty \tau K(\tau)d\tau| \ll 1$. To analyze this condition analytically is rather complicated. Our numerical calculations show that the approximate condition of applicability is $|V_{1,2}| \lesssim (\gamma_1+\gamma_2)$. Note that the same condition is also required for the exact solutions of Eqs. (7)–(9) to be approximated by Eqs. (21) and (22). (See [22] for details.)

2. Single collective diagonal noise

In the case of a single collective noisy environment, acting on both the donor and acceptor, the rate Γ in Eq. (23) has the form

$$\Gamma=\frac{8V^2\mu^2}{\gamma((\mu^2-\nu^2)^2+4\nu^2)}. \tag{25}$$

Substituting $\mu=d/\gamma$ and $\nu=\varepsilon/\gamma$, we obtain

$$\Gamma=\frac{8\gamma|V_{12}|^2d^2}{(d^2-\varepsilon^2)^2+4\gamma^2\varepsilon^2}, \tag{26}$$

where $d=(\lambda_1-\lambda_2)\sigma$ denotes the amplitude of the noise. As one can see, the rate Γ reaches its maximum,

$$\Gamma_{\max}=\frac{4\gamma|V_{12}|^2}{\sqrt{\varepsilon^4+4\gamma^2\varepsilon^2}-\varepsilon^2}, \tag{27}$$

at the "resonance" amplitude of the noise,

$$d_{\mathrm{res}}=(\varepsilon^4+4\gamma^2\varepsilon^2)^{1/4}. \tag{28}$$

(See also [9,10].) When the amplitude of the noise is far from the resonance value, the rate Γ becomes very small.

3. The "nonlinear" regime of electron transfer

The dependence of the ET rate Γ in Eq. (26) on the amplitude d of the noise (the external random force) is a nonlinear one. Indeed, the amplitude d appears in Γ in both the numerator and the denominator. Suppose that the value of d is small $(d \ll \varepsilon)$. In this case, $\Gamma \approx 8\gamma|V_{12}|^2/\varepsilon^2(\varepsilon^2+4\gamma^2)$, and the rate is proportional to the intensity of the external random process. So, in this "linear" regime (small d), there are no resonances in the $\Gamma(d)$ behavior. In the opposite case of strong noise $(d \gg \varepsilon)$, the ET rate is $\Gamma \approx 8\gamma|V_{12}|^2/d^2$, and it decreases as d increases. We can say that the strong noise does not allow the electron to move from the donor to the acceptor, a kind of ET Zeno effect. Only for intermediate noise amplitudes d does the "resonance" in the behavior of $\Gamma(d)$ take place. In this sense, the regime of the ET is a nonlinear one. A similar situation occurs when two uncorrelated noises are applied to the system. In this case, two "interacting nonlinear resonances" occur.

There are two limiting cases in which the expression for $\Gamma_{\max}$ can be simplified. (1) $\varepsilon \gg 2\gamma$. In this case, $\Gamma_{\max} \approx 2|V_{12}|^2/\gamma$. (2) $\varepsilon \ll 2\gamma$. In this case, $\Gamma_{\max} \approx 2|V_{12}|^2/\varepsilon$. An approximate condition for applicability of Eq. (26) for the rate is $|V_{12}| \lesssim \gamma,d$.

B. Results of numerical simulations

In the numerical simulations, it is convenient to measure the energy parameters in units of ps^{-1}, while time is measured in ps. Then the energy $\varepsilon = 1\ \mathrm{ps}^{-1} \approx 0.66$ meV.

In Fig. 2, we show the rate Γ defined by Eq. (26) (for a single noise), as a function of the amplitude of noise d and the correlation rate of noise (inverse correlation time) γ. As one can see, Γ reaches its maximum value at the resonance

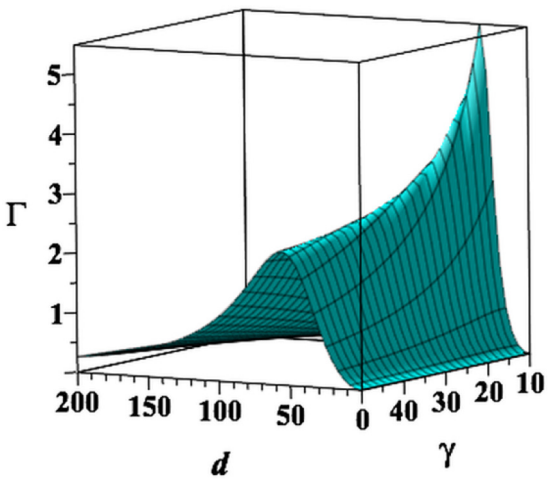

FIG. 2. (Color online) Dependence of the rate Γ in Eq. (26) on the noise amplitude d and the correlation rate γ. Parameters: $V_{12}=5$, $\varepsilon=30$.

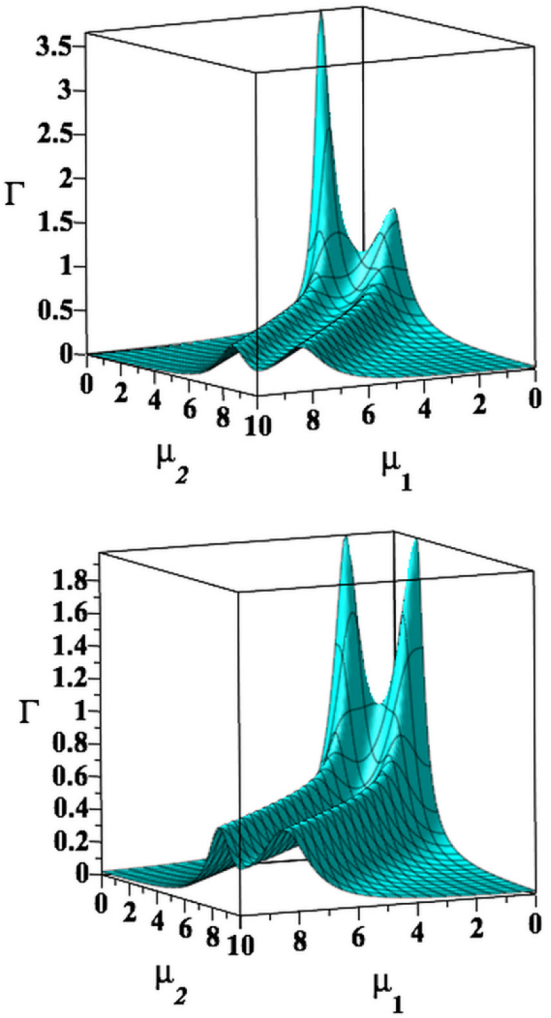

FIG. 3. (Color online) Asymptotic rate Γ of Eq. (23) vs the dimensionless amplitudes of two uncorrelated noises μ_1 and μ_2. Parameters: $V_{12} = 3$, $\varepsilon = 30$. Top: $\gamma_1 = 5$, $\gamma_2 = 15$. Bottom: $\gamma_1 = \gamma_2 = 10$.

amplitude of the noise $d_{\rm res}$ given by Eq. (28). At the same time, as one can see from Eq. (28), for a given value of the redox potential ε the value of $\Gamma_{\rm max}$ depends on γ. This behavior is demonstrated in Fig. 2, for $\varepsilon = 50$, $|V_{1,2}| = 5$, and $10 \leq \gamma \leq 50$. One case see that for these parameters $\Gamma_{\rm max} \lesssim 6\ {\rm ps}^{-1}$.

For two uncorrelated noises, the rate Γ in Eq. (23) is shown in Fig. 3 as a function of two dimensionless amplitudes of noise μ_1 and μ_2. As one can see, two "interacting" resonances are present. The amplitudes of these resonances depend on the values of $\mu_{1,2}$. These resonances can be either nonsymmetric, as in Fig. 3 (top), for different correlation rates $\gamma_1 = 5$ and $\gamma_2 = 15$, or symmetric, as in Fig. 3 (bottom), for equal correlation rates $\gamma_{1,2} = 10$. Note that in both cases $\gamma_1 + \gamma_2 = 20$. For these chosen parameters, $\Gamma_{\rm max} \lesssim 3.6\ {\rm ps}^{-1}$.

1. Weakly and strongly coupled dimers

The donor-acceptor system shown in Fig. 1 represents a coupled dimer (realized, for example, by two coupled chlorophyll molecules.) This dimer can be either weakly or strongly coupled. Let us introduce the parameter $\mu_d = |V_{12}/\varepsilon|$.

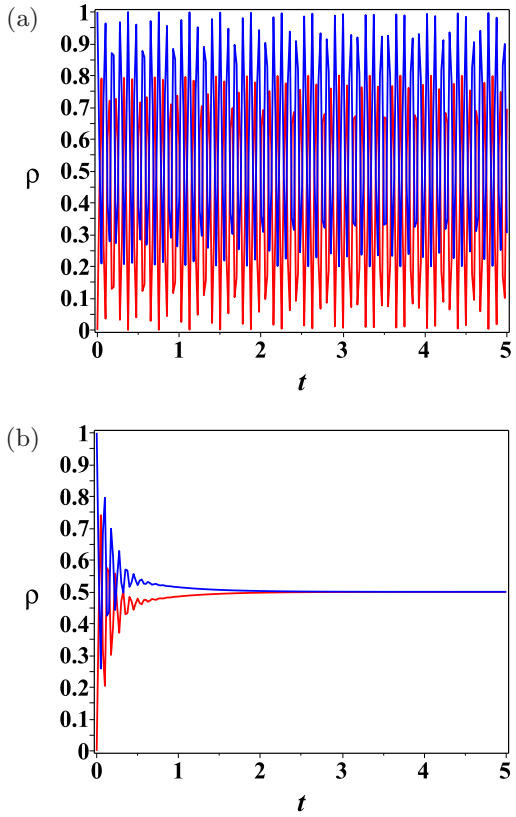

FIG. 4. (Color online) Strongly coupled dimer ($\mu_d = 1$). Time dependence (in picoseconds) of the density matrix components: $\rho_{11}(t)$ (blue) and $\rho_{22}(t)$ (red). Parameters: $V_{12} = 30, \varepsilon_1 = 60, \varepsilon_2 = 30$, $\gamma_1 = 10$, $\gamma_2 = 15$. (a) $d_1^{(1)} = 10$, $d_2^{(1)} = 10$, $d_1^{(2)} = 0$, $d_2^{(2)} = 0$; (b) $d_1^{(1)} = 10, d_2^{(1)} = 0, d_1^{(2)} = 0, d_2^{(2)} = 10$. Initial conditions: $\rho_{11}(0) = 1$, $\rho_{22}(0) = 0$.

It is easy to see that, when $\mu_d \ll 1$, both eigenstates $|u_+\rangle$ and $|u_-\rangle$ of the Hamiltonian $\mathcal{H}_0$ in (2) become close to the unperturbed states $|u_1\rangle$ and $|u_2\rangle$ when $V_{12} = 0$. In this case, we say that the dimer is "weakly coupled." The dimer is called "strongly coupled" when the value of μ_d is not too small. We can say that the dimer is strongly coupled when $\mu_d \gtrsim 1$.

In Figs. 4–7, we present the results of the numerical simulations of the dynamical behavior of the system shown in Fig. 1, for different parameters, and for both correlated and uncorrelated noisy environments. All simulations were performed using the exact system of equations (7)–(9). In Fig. 7, we also compare the exact results with the corresponding approximate solutions. (In [22], more details of the comparison of the exact and approximate solutions are presented.) We also consider weakly and strongly coupled dimers. For simplicity, in all cases, the initial conditions were chosen when the donor was populated: $\rho_{11}(0) = 1$, $\rho_{22}(0) = \rho_{12}(0) = 0$.

In Fig. 4(a), a single correlated noise, corresponding to $a = 1$, is applied to a strongly coupled dimer ($\mu_d = 1$). In this case, the amplitudes of the noises acting on donor and acceptor are equal, $d_1^{(1)} = d_2^{(1)} = 10$. So the effective noise acting on the system is absent: $d^{(1)} = d_1^{(1)} - d_2^{(1)} = 0$. This regime is easy to understand, as the matrix $\mathcal{V}_a$ in Eq. (1) becomes the unit matrix. In this case, the dynamics of the system exhibits Rabi oscillations. Because the matrix element is equal

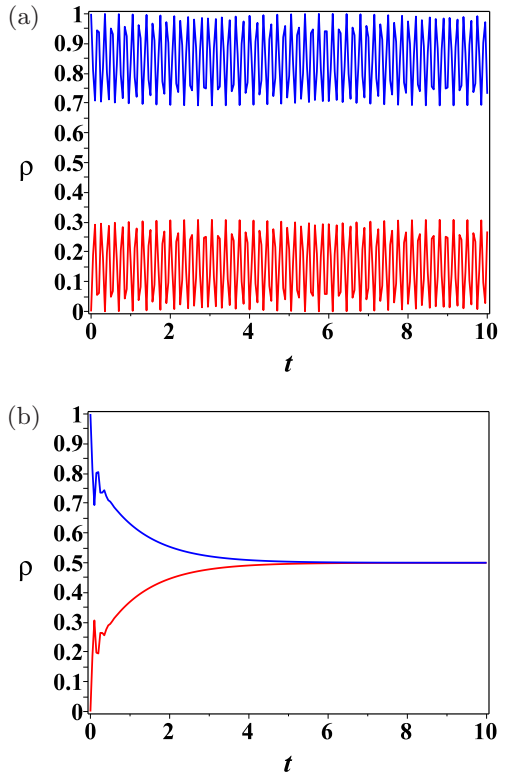

FIG. 5. (Color online) Time dependence (in picoseconds) of the density matrix components: $\rho_{11}(t)$ (blue) and $\rho_{22}(t)$ (red). Parameters: $V_{12} = 10$, $\varepsilon_1 = 60, \varepsilon_2 = 30$, $\gamma_1 = 10$, $\gamma_2 = 15$. (a) $d_1^{(1)} = 10$, $d_2^{(1)} = 10$, $d_1^{(2)} = 0$, $d_2^{(2)} = 0$, (b) $d_1^{(1)} = 10$, $d_2^{(1)} = 0$, $d_1^{(2)} = 0$, $d_2^{(2)} = 10$. Initial conditions: $\rho_{11}(0) = 1$, $\rho_{22}(0) = \rho_{12}(0) = 0$.

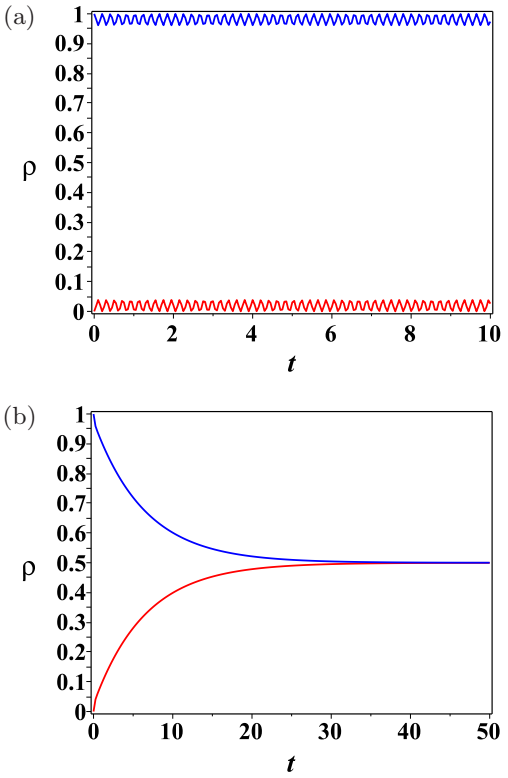

FIG. 6. (Color online) Weakly coupled dimer ($\mu_d = 0.1$). Time dependence (in picoseconds) of the density matrix components: $\rho_{11}(t)$ (blue) and $\rho_{22}(t)$ (red). Parameters: $V_{12} = 3$, $\varepsilon_1 = 60, \varepsilon_2 = 30$, $\gamma_1 = 10, \gamma_2 = 15$. (a) $d_1^{(1)} = 10, d_2^{(1)} = 10, d_1^{(2)} = 0, d_2^{(2)} = 0$; (b) $d_1^{(1)} = 10$, $d_2^{(1)} = 0$, $d_1^{(2)} = 0$, $d_2^{(2)} = 10$. Initial conditions: $\rho_{11}(0) = 1$, $\rho_{22}(0) = \rho_{12}(0) = 0$.

to the redox potential $V_{1,2} = \varepsilon = 30$, the Rabi oscillations have large amplitude. The situation changes significantly when two uncorrelated noises with the same amplitudes, $d_1^{(1)} = 10$ (applied to the donor) and $d_2^{(2)} = 10$ (applied to the acceptor), influence the same dimer. [See Fig. 4(b).] In this case, the dynamics experiences rapid relaxation and saturates $[\rho_{1,2}(t) \to 1/2]$ at approximately $t_s \approx 2$ ps. We can conclude that, in this case, two uncorrelated noises (environments) with equal amplitudes are more effective in assisting the ET than a single correlated noise with the same amplitude. Similar results are shown in Fig. 5 for the intermediately coupled dimer ($\mu_d = 1/3$). In this case, the amplitude of the Rabi oscillations in Fig. 5(a) decreases, and the saturation time in Fig. 5(b) increases, $t_s \approx 6$ ps. In both cases shown in Figs. 4(b) and 5(b) the electron transfer dynamics is accompanied by coherent oscillations of the populations $\rho_{11}(t)$ and $\rho_{22}(t)$. In Fig. 6, the case of a weakly coupled dimer is demonstrated, for $\mu_d = 0.1$ and for the same amplitudes of the noisy environments as in Figs. 4 and 5. As one can see, the amplitude of the Rabi oscillations in Fig. 6(a) decreases significantly (to less than 0.05), and the saturation time of the ET in Fig. 6(b) increases significantly, $t_s \approx 35$ ps. The populations $\rho_{11}(t)$ and $\rho_{22}(t)$ do not experience visible oscillations in this case.

In Fig. 7, we show the dynamics of the ET for two noises, which act on both donor and acceptor, but with different amplitudes and interaction constants. The solid curves correspond to the solutions of the exact equations (7)–(9). The dashed curves correspond to the approximate solutions given by Eqs. (21) and (22). The initial conditions are the same for all cases presented in Fig. 7: $\rho_{11}(0) = 1$,

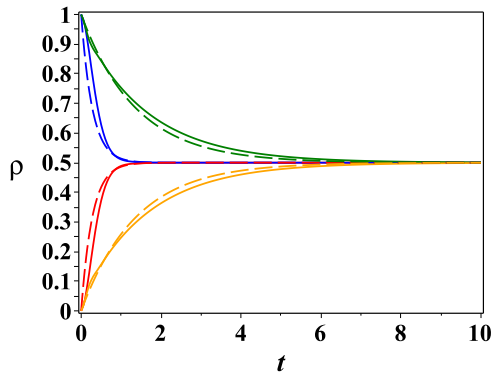

FIG. 7. (Color online) Weakly coupled dimer ($\mu_d = 0.1$). Time dependence (in picoseconds) of the density matrix components: $\rho_{11}(t)$ (blue and green curves) and $\rho_{22}(t)$ (red and orange curves). Choice of parameters: $V_{12} = 3$, $\varepsilon_1 = 60, \varepsilon_2 = 30$, $\gamma_1 = 5$, $\gamma_2 = 15$. Blue and red curves: $d_1^{(1)} = 20$, $d_2^{(1)} = -10$, $d_1^{(2)} = 0$, $d_2^{(2)} = 0$, $\Gamma = 3.6$ ($\mu_1 = 1.5; \mu_2 = 0$). Green and orange curves: $d_1^{(1)} = 20$, $d_2^{(1)} = 0$, $d_1^{(2)} = 0$, $d_2^{(2)} = -10$, $\Gamma = 0.73$ ($\mu_1 = 1; \mu_2 = 0.5$). Solid curves correspond to the solutions of the exact Eqs. (7)–(9). Dashed curves correspond to the approximate solutions given by Eqs. (21) and (22). Initial conditions: $\rho_{11}(0) = 1$, $\rho_{22}(0) = \rho_{12}(0) = 0$.

$\rho_{22}(0) = \rho_{12}(0) = 0$. Blue and red curves correspond to the noise amplitudes $d_1^{(1)} = 20$, $d_2^{(1)} = -10$, $d_1^{(2)} = 0$, $d_2^{(2)} = 0$. In this case, even though two noises are present in the system, the second noise (with $a = 2$) has zero constants of interaction with both the donor and acceptor: $\lambda_{1,2}^{(2)} = 0$. So effectively only one collective noise (with $a = 1$) acts on both the donor and acceptor. The dimensionless amplitudes of the noise are $(\mu_1 = 1.5, \mu_2 = 0)$, and the ET rate is $\Gamma = 3.6$.

Green and orange curves correspond to the amplitudes of noise $d_1^{(1)} = 20$, $d_2^{(1)} = 0$, $d_1^{(2)} = 0$, $d_2^{(2)} = -10$. In these case, both noises act on the system. The dimensionless amplitudes of the noise are $(\mu_1 = 1, \mu_2 = 0.5)$, and the ET rate is $\Gamma = 0.73$. The presented ET rates correspond to the results shown in Fig. 3. As one case, for the chosen parameters, the results of the approximate solutions (dashed curves) are in good agreement with the results of the exact equations (solid curves). As our results demonstrate, the saturation time depends significantly on (i) the presence of collective or independent (uncorrelated) noises acting on the donor and acceptor, (ii) the amplitudes of the noises, and (iii) the interaction constants with the noises. Indeed, for the parameters chosen in Fig. 7, for the blue and red curves, the saturation time is $t_{\rm sat} \approx 1.8$ ps. For the parameters chosen for the green and orange curves, the saturation time is $t_{\rm sat} \approx 8$ ps.

IV. CONCLUSION

When modeling the primary quantum exciton transfer processes in photosynthetic complexes, two major problems occur. The first is related to strong pigment-protein interactions. The second problem is related to the large number of pigments (or light-sensitive sites) in the light-harvesting complexes. This results in a multiscale electron transfer dynamics and in the necessity to develop adequate coarse-grained procedures. Moreover, the number N of light-sensitive pigments in the subcomplexes of plants and algae is neither small nor large, but rather of an intermediate value $N \approx 10$–20 [1,2]. Then it is difficult to apply the well-developed methods from solid state physics which are used either for rare impurities or for systems with electron band structures.

In this situation, it is useful to design a simple and "exactly solvable" (at least numerically) quantum model which can be used to describe the electron transfer in these complex biological systems. Such a model, which is reduced to an exact closed system of first-order linear differential equations with constant coefficients, is described in this paper. This model can be applied for rather general photosynthetic complexes and for any values of the pigment-protein coupling constants. Note that the term "exactly solvable" which we use here is rather conditional. It means that the model consists of a closed system of ordinary differential equations with constant coefficients, which can be easily solved numerically. (See also the close approach used in [7,8].) Our model also includes different correlated and uncorrelated random telegraph processes, acting on different sites. This allows one to analyze in a straightforward way the dependences of the electron transfer dynamics on both the amplitudes and correlation times of random processes. In particular, it is demonstrated that the influence of noise on the electron transfer reveals a resonant character, which will allow one to design photosynthetic complexes with optimal electron transfer properties.

We demonstrated that uncorrelated protein fluctuations can either increase or decrease the electron transfer rates. We also derived analytical expressions for the ET rates and for the evolution of the density matrix elements, which approximate the exact solutions for large time intervals for a wide range of parameters.

Although our model is relevant to describing some important effects considered in the paper, it does not include many important effects, such as temperature dependencies, the internal structures of the electron sites (which usually are represented by light-sensitive chlorophyll and carotenoid molecules), multiexciton or multielectron states, etc.

Our approach can easily be applied for many concrete light-harvesting complexes and reaction centers. The solutions which follow from our model can be used for developing adequate coarse-grained procedures and for comparison with the results of different approximations and perturbation approaches. Our results can also be used for engineering the protein environment to achieve desired properties for the ET dynamics. In order to verify the properties of the protein environment, standard molecular dynamics methods can be used to simulate the time-dependent correlation functions between different electron sites. The generalization of our approach for thermal protein environments is one focus of our future research. One way to do this is to develop a perturbation theory not by the constants of interactions between the electron sites and the protein fluctuations, but by the matrix elements of the interactions between different electron sites. This research is now in progress.

ACKNOWLEDGMENTS

This work was carried out under the auspices of the National Nuclear Security Administration of the U.S. Department of Energy at Los Alamos National Laboratory under Contract No. DE-AC52-06NA25396. A.I.N. acknowledges support from the CONACyT Grant No. 15349.

[1] G. Panitchayangkoon, D. Hayes, K. A. Fransted, J. R. Caram, E. Harel, J. Wen, R. E. Blankenship, and G. S. Engel, Long-lived quantum coherence in photosynthetic complexes at physiological temperature, Proc. Natl. Acad. Sci. USA **107**, 12766 (2010).

[2] D. I. G. Bennett, K. Amarnath, and G. R. Fleming, A structure-based model of energy transfer reveals the principles of light harvesting in photosystem II supercomplexes, J. Am. Chem. Soc. **135**, 9164 (2013).

[3] R. Marcus and N. Sutin, Electron transfers in chemistry and biology, Biochim. Biophys. Acta **811**, 265 (1985).

[4] D. Xu and K. Schulten, Coupling of protein motion to electron transfer in a photosynthetic reaction center: Investigating the

low temperature behavior in the framework of the spin-boson model, Chem. Phys. **182**, 91 (1994).

[5] J. Jortner, Temperature dependent activation energy for electron transfer between biological molecules, J. Chemical. Phys. **87**, 2090 (1987).

[6] I. Rips and J. Jortner, Dynamic solvent effects on outer-sphere electron transfer, J. Chem. Phys. **64**, 4860 (1976).

[7] R. Pinčák and M. Pudlak, Noise breaking the twofold symmetry of photosynthetic reaction centers: Electron transfer, Phys. Rev. E **64**, 031906 (2001).

[8] M. Pudlak and R. Pinčák, Modeling charge transfer in the photosynthetic reaction center, Phys. Rev. E **68**, 061901 (2003).

[9] S. Gurvitz, A. I. Nesterov, and G. P. Berman, Noise-assisted quantum electron transfer in multi-level donor-acceptor system, arXiv:1404.7816 [physics.bio-ph].

[10] G. P. Berman, A. I. Nesterov, S. Gurvitz, and R. T. Sayre, Possible role of interference and sink effects in nonphotochemical quenching in photosynthetic complexes, arXiv:1412.3499 [physics.bio-ph].

[11] M. Pudlak, Electron transfer driven by conformational variations, J. Chem. Phys. **108**, 5621 (1998).

[12] M. Pudlak, Primary charge separation in the bacterial reaction center: Validity of incoherent sequential model, J. Chem. Phys. **118**, 1876 (2003).

[13] S. Westenhoff, D. Palecek, P. Edlund, P. Smith, and D. Zigmantas, Coherent picosecond exciton dynamics in a photosynthetic reaction center, J. Am. Chem. Soc. **134**, 16484 (2012).

[14] T. G. Dewey and J. G. Bann, Biophys, Protein dynamics and 1/f noise, J. Biophys Society **63**, 594 (1992).

[15] B. H. McMahon, P. W. Fenimore, and M. X. LaBute, Fluctuations and noise in biological, biophysical, and biomedical systems, Proc. SPIE, **5110**, 10 (2003).

[16] M. Pudlak, Effect of the conformational transitions on electron transfer in biological systems, Physica A **341**, 444 (2004).

[17] M. Pudlak, K. N. Pichugin, R. G. Nazmitdinov, and R. Pincak, Quantum nonequilibrium approach for fast electron transport in open systems: Photosynthetic reaction centers, Phys. Rev. E **84**, 051912 (2011).

[18] S. S. Skourtis, D. H. Waldeck, and D. N. Beratan, Fluctuations in biological and bioinspired electron-transfer reactions, Annu. Rev. Phys. Chem. **61**, 461 (2010).

[19] A. I. Nesterov, G. P. Berman, and A. R. Bishop, Non-Hermitian approach for modeling of noiseassisted quantum electron transfer in photosynthetic complexes, Fortschr. Phys. **61**, 95 (2013).

[20] J. M. Moix and J. Cao, A hybrid stochastic hierarchy equations of motion approach to treat the low temperature dynamics of non-Markovian open quantum systems, J. Chem. Phys. **139**, 134105 (2013).

[21] V. Abramavicius and D. Abramavicius, Excitation transfer pathways in excitonic aggregates revealed by the stochastic Schrdinger equation, J. Chem. Phys. **140**, 065103 (2013).

[22] See Supplemental Material at http://link.aps.org/supplemental/10.1103/PhysRevE.91.042702 for mathematical details of our approach.

[23] V. Klyatskin, *Dynamics of Stochastic Systems* (Elsevier, Amsterdam, 2005).

[24] A. I. Nesterov, G. P. Berman, J. M. Sánchez Martinez, and R. Sayre, Noise-assisted quantum electron transfer in photosynthetic complexes, J. Math. Chem. **51**, 1 (2013).

[25] J. Bergli, Y. M. Galperin, and B. L. Altshuler, Decoherence in qubits due to low-frequency noise, New J. Phys. **11**, 025002 (2009).

[26] A. I. Nesterov and G. P. Berman, Modeling of low- and high-frequency noise by slow and fast fluctuators, Phys. Rev. A **85**, 052125 (2012).